Received: 18 February 2018 | Revised: 26 June 2018 | Accepted: 27 June 2018

DOI: 10.1002/nag.2846

RESEARCH ARTICLE

WILEY

Intricacies in three-dimensional limit analysis of earth slopes

Dowon Park | Radoslaw L. Michalowski

Department of Civil and Environmental Engineering, University of Michigan, Ann Arbor, MI, U.S.A.

Correspondence
Radoslaw L. Michalowski, Department of Civil and Environmental Engineering, University of Michigan, 2028 G.G. Brown Bldg, Ann Arbor, MI 48109-2125, U.S.A.
Email: rlmich@umich.edu

Funding information
Division of Civil, Mechanical, and Manufacturing Innovation, Grant/Award Number: 1537222; National Science Foundation

Summary

Analyses of three-dimensional slope failures can be elaborate because of the complexity owed to the geometry of the failure mechanism that needs to conform to an admissible kinematics of the slope collapse. This admissibility is imposed by the soil limit state condition, the normality plastic flow rule, and the boundary conditions. The kinematic approach of limit analysis is employed, and a rotational 3D slope failure is revisited. The study leads to the conclusion that some geometric constraints used in previous studies limit the range of admissible mechanisms resulting in overestimating stability factors. A set of results is presented that was obtained using an algorithm that allowed eliminating limitations present in previous studies. The largest improvements in the solutions were found for undrained failures of narrow slopes. For a 30° slope limited in width by the width-to-height ratio of 0.6, the stability factor calculated in previous studies overestimated the current calculations by nearly 39%. This overestimation is smaller for drained failures, and it drops significantly with an increase in the width of the failure mechanism.

KEYWORDS

landslides, limit analysis, plasticity analysis, slope stability

1 | INTRODUCTION

Safety assessment of slopes is an important exercise in geomechanics. Typical stability analyses involve two-dimensional considerations, but in many cases a three-dimensional analysis is called for. For example, excavation slopes or soil slopes limited in width by a rock outcrop require three-dimensional analyses if an accurate assessment is needed.

Observations of failure surfaces in clays were documented as early as 1846 by Collin,[1] but 2D analyses of stability were not introduced until the 20th Century (Fellenius,[2] Taylor,[3] Drucker and Prager[4]). Three-dimensional analyses of stability of slopes can be grouped into traditional limit equilibrium methods, limit analysis, and numerical approaches

Notation: D, -rate of internal work (dissipated work); H, -slope height; L, -area of velocity discontinuity surface; N_f, -stability factor $\gamma H/c$; N_n, -stability number $c/\gamma H$; R, -radius of the nonlinear cone cross section; S, -area of a surface; T_i, -stress vector; V, -volume of the mechanism; W_s, -rate of work of inertial (seismic) forces; W_u, -rate of work of pore water pressure on volumetric strain of soil; W_γ, -rate of work of soil weight; X_i, -distributed load vector; c, -cohesion of bonded soil; k_h, -coefficient of horizontal acceleration; r, -radius of the failure surface at the central cross section; r', -upper radius of the conical surface; r_c, -radius of the curvilinear cone centerline; r_s, -radius defining the contour of the slope; r_u, -pore water pressure coefficient; s_u, -undrained shear strength; $[v]_i$, -velocity jump vector on a failure surface; v_i, -velocity vector; v, -magnitude of the velocity vector; γ, -unit weight; $\dot{\varepsilon}_{ij}^{pl}$, -plastic strain rate tensor; θ, -angular coordinate; ρ, -radial coordinate; σ_{ij}, -stress tensor; ϕ, -internal friction angle; ω, -angular velocity

such as finite element analysis. The 3D analyses were first developed for undrained failures, as the mechanisms in incompressible materials are easier to construct (Baligh and Azzouz,[5] Gens et al[6]). The early 3D analyses for pressure-dependent materials were based on traditional limit-equilibrium slice methods extended to 3D failures.[7-9] Drescher[10] presented a one-block collapse mechanism in a pressure-dependent material, while a 3D multi-block limit analysis was presented by Michalowski.[11] Leshchinsky et al[12] developed a rotational mechanism in pressure-dependent materials using a limit equilibrium approach, with a kinematically admissible mechanism arrived at through a variational approach. The outcome of that approach was equivalent to kinematic limit analysis. A rotational mechanism was also considered by De Buhan and Garnier.[13] A 3D rotational mechanism was postulated by Michalowski and Drescher,[14] which was used in a series of related publications.[15-18] More recently, the variational approach to finding the critical failure surface was revisited by Zhang et al.[19] While purely rotational mechanisms may not necessarily be the most critical,[20] the rotational collapse appears to be more critical than other 3D mechanisms suggested throughout the literature.

Finite element analysis of two-dimensional and three-dimensional slope failures was considered throughout the literature,[21-24] while the finite element implementation of limit analysis for the purpose of safety assessment of slopes (3D) was also presented in recent years.[25,26] Numerical approaches have advantages of accounting for soil inhomogeneities and not having to predetermine the mode of failure. However, when it comes to assessment of stability, they also come with some disadvantages. For example, at the time of stability loss, the solution does not converge in the finite element analyses, and a lack of convergence in a prescribed number of iterations is often considered as a criterion for reaching instability. This is not an elegant procedure, although it has proved to be effective. An advantage of using finite element implementation of limit analysis is in its ability to find both the upper and lower bounds to the true solution, whereas the more common "analytical" method can be used effectively only with the kinematic approach of limit analysis. It is not uncommon, however, that a well-chosen mechanism in the analytical approach can yield a better solution to a stability measure than the finite element approach.[15,19,27]

The slope failure mechanism considered in this paper can be applied to slopes with arbitrary limitations on the slope width. Failing mass in natural slopes, particularly hillside slopes, is often constrained by bedrock,[22,23] while the kinematics can also be affected by a rock outcrop and the terrain topography.[28] These kinematic constraints are not considered in this paper, although the limitation on the depth of the mechanism can be easily introduced into the analysis by placing a proper constraint on the optimization process.

This paper's focus is on the kinematic approach of limit analysis in slope stability considerations. In particular, the rotational failure mechanism is revisited to assess the source of differences in the outcomes of analyses coming from different studies but based on the same mechanism of failure. The kinematic approach is described briefly first, followed by the description of the 3D collapse mechanism and the geometric intricacies in the mechanism that are likely to be the source of discrepancies in the results published throughout the literature.

2 | KINEMATIC LIMIT ANALYSIS APPLIED TO SLOPES

2.1 | Material model and limitations of the method

Limit analysis has been widely applied in stability of structures and plastic forming of metals (Hill[29]), followed by applications in geotechnical engineering (Drucker and Prager,[4] Salençon,[30] Chen[31]). The fundamental assumption in the analysis is the perfectly plastic behavior of the material, described by a convex yield condition and the normality plastic flow rule. This assumption allows using the postulate of maximum plastic work, which, in turn, allows proving the theorems of limit analysis. The yield criteria for metals are pressure independent, and the outcome of application of the normality flow rule is incompressible plastic flow, which is consistent with experimental observations for metals. With yielding of geomaterials exhibiting pressure dependency, the associative (normality) flow rule leads to dilative plastic deformation, typically overestimating the observed volumetric strains. Application of the non-associative flow rule to geomaterials was considered early by Mróz.[32]

Plastic deformation of geomaterials does not conform to the normality flow rule (typically, normality law overestimates volumetric deformation), and the reason for using associativity in limit analysis is purely mathematical: without the normality flow rule, the theorems of limit analysis cannot be proved. Hence, the associativity of plastic flow is needed for the solutions to boundary value problems to be strict lower or upper bounds to a true solution. The kinematic approach is used in this paper, and we refer to the theorem used as the *kinematic theorem of limit analysis*. This theorem is more commonly referred to as the *upper-bound theorem*, but this term is ambiguous. This is because the outcome of application of this theorem can be either an upper bound, for instance, when the active limit load is calculated,

or a lower bound when a passive force (reaction) is sought. Whether the material obeys associativity or not, it can be proved that this approach yields a rigorous bound to the true solution. This was shown by Redenkovic[33] and, with an intuitive graphical interpretation, by Palmer.[34] For this very same reason, the normality sliding rule was used in problems with frictional boundary conditions, where the true sliding rule made the analytical solution not possible (Collins,[35] Mróz and Drescher,[36] Michalowski and Mróz[37]).

Limit analysis is an approximate method, but it yields a rigorous bound to the true solution. However, not every stability problem can be addressed with limit analysis. This is because the theorems of limit analysis, strictly, only allow calculations of a bound on an integral of the rate of work of the unknown load, and not every boundary condition allows extracting the load from this integral. For instance, a limit force on a footing can be found using limit analysis if the boundary condition is given as a rigid translation of the footing, but if the kinematic boundary condition is given in terms of rotation, one can only find a limit moment, but not the force. This is one of the limitations of the method. Another limitation follows from the integral form of the work rate balance, making it possible to find limit forces (or moments), but not their distributions. The stress field cannot be determined either. Finally, only incipient stability problems can be tackled, and no displacements or progressive failure can be tracked with confidence. The formulation of the slope stability problem involves a static boundary condition, most typically a stress-free boundary.

2.2 | Equilibrium in kinematic limit analysis

The common form of the work rate balance equation used in the kinematic approach can be written as

$$\int_V \sigma_{ij}\dot{\varepsilon}_{ij}^{pl} dV + \int_L T_i \,[v]_i dL = \int_S T_i v_i dS + \int_V X_i v_i dV \tag{1}$$

where the two terms on the left-hand side represent the rate of plastic work dissipation (internal work), and the two terms on the right-hand side depict the rate of external work (see Notation for explanation of symbols). The first term on the left-hand side represents the work dissipation rate in volume V (due to plastic strain within the volume), and the second one is the dissipation on kinematic discontinuity surfaces L. The first term on the right-hand side represents the work rate of traction vector T_i on boundary S of the mechanism, and the second term is the work rate of distributed forces X_i in volume V (eg, gravity load). The kinematic theorem indicates that the left-hand side (the rate of plastic work) is not smaller than the work rate of the true external loads (right-hand side) in any kinematically admissible mechanism of plastic deformation. Manipulation of Equation (1) allows one to find a rigorous bound on an unknown limit load. For example, in the case of a footing on boundary S, one could find an upper bound to the footing limit load (integral of traction T_i on boundary S), if the velocity on this boundary, v_i, was constant (rigid translation). However, the left-hand side of the balance in Equation (1) is calculated based solely on the yield condition and normality flow rule applied to the postulated failure mechanism; hence, in general, stress field σ_{ij} does not satisfy equilibrium. Therefore, Equation (1) cannot be considered the principle of virtual work for a deformable body. For a rigid-body translational mechanism, however, the first term in Equation (1) is zero, and the remaining terms assume the form of the principle of virtual work for a rigid-body mechanism. Consequently, the equilibrium of forces (not stresses) will be enforced if Equation (1) is used to calculate an unknown force in a rigid block mechanism. This was shown explicitly by Michalowski[11] (see also Drescher and Detournay[38] and Salençon[39]). Similarly, global equilibrium of moments will be enforced in a rigid rotational mechanism.

3 | ROTATIONAL 3D FAILURE MECHANISM

There are relatively few limit analysis solutions to slope stability that include three-dimensional mechanisms of failure in pressure-dependent materials. The early ones are the translational mechanisms, including the classical wedge-type failure often exploited in rock mechanics with a limit equilibrium type of solution,[40] a single-block mechanism by Drescher,[10] and a multi-block mechanism by Michalowski.[11] A rotational mechanism of slope failure was used in limit analysis by De Buhan and Garnier[13] and by Michalowski and Drescher.[14] A special case of the mechanism postulated by Michalowski and Drescher[14] was arrived at earlier by Leshchinsky et al,[12] and it was exploited further more recently by Zhang et al.[19] The primary method used by Leshchinsky et al[12] was the limit equilibrium method with the variational approach used to optimize the mechanism of failure. The kinematics in these rotational mechanisms is plane, but the geometry of the failure surface is three-dimensional.

3.1 | Curvilinear cone failure surface

A curvilinear cone failure surface was postulated in Michalowski and Drescher[14] by requiring that all radial cross sections of the cone are circles, and the trace of the cone on the plane of symmetry is governed by two log-spirals

$$r(\theta) = r_0\, e^{(\theta-\theta_0)\tan\phi} \tag{2}$$

$$r'(\theta) = r_0'\, e^{-(\theta-\theta_0)\tan\phi} \tag{3}$$

with r_0 and r_0' illustrated in Figure 1. Effectively, this surface is generated by revolving a circle of variable radius $R(\theta)$

$$R(\theta) = \frac{r(\theta)-r'(\theta)}{2} \tag{4}$$

about an axis passing through center O. The central line of the generated curvilinear cone is described by radius $r_c(\theta)$

$$r_c(\theta) = \frac{r(\theta)+r'(\theta)}{2}. \tag{5}$$

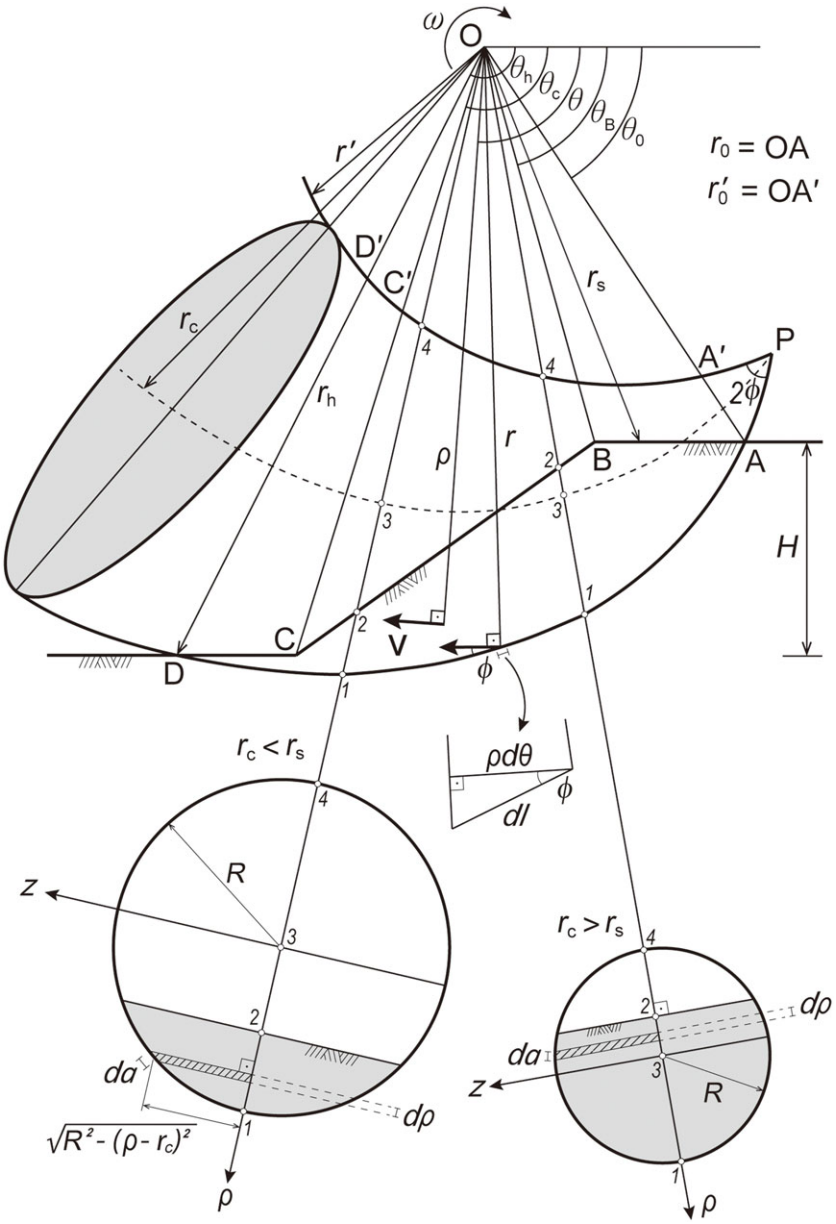

FIGURE 1 Three-dimensional rotational failure mechanism generated by revolving a circle of increasing diameter about an axis passing through point O

With the material strength described by the Mohr-Coulomb criterion, such a surface forms an admissible failure surface in the rotational mechanism as it assures that the vector of velocity is inclined at internal friction angle ϕ to the conical surface at every point of the surface. Such surface was earlier postulated in a translational mechanism under square and rectangular footings[41] and was more recently used to analyze passive pressure on retaining walls.[42] This surface can also be modified to account for pressure-dependent geomaterials with nonlinear strength envelopes.[43,44] Since its inception, the 3D slope failure mechanism postulated[14] was adopted in many slope stability studies. The mathematical description of this mechanism is redeveloped here to remove some of the restrictions, and to allow for finding more critical failure surfaces. This new and more general algorithm is also simpler than the one originally presented.[14]

In the polar co-ordinate system ρ,θ the contour of the slope can be described as a piece-wise function $r_s(\theta)$ (see Figure 1)

$$r_s(\theta) = \begin{cases} \dfrac{r_0 \sin\theta_0}{\sin\theta}\ , & \theta_0 < \theta \le \theta_B \\ \dfrac{r_h \sin(\beta+\theta_h)}{\sin(\beta+\theta)}\ , & \theta_B < \theta \le \theta_C \quad (\theta_C = \theta_h \text{ for toe failure}) \\ \dfrac{r_h \sin\theta_h}{\sin\theta}\ , & \theta_C < \theta \le \theta_h \quad (\text{Below-toe only}) \end{cases} \tag{6}$$

where

$$r_h = r_0 e^{(\theta_h - \theta_0)\tan\phi} \tag{7}$$

and

$$\theta_B = \arctan\left(\frac{r_h \sin\theta_h - H}{r_h \cos\theta_h + H\cot\beta}\right) \tag{8}$$

and θ_0, θ_h, and θ_C are independent geometrical parameters ($\theta_C = \theta_h$ for toe failures). The mechanism in Figure 1 differs from that in Michalowski and Drescher[14] in the following detail: the center line $r_c(\theta)$ of the curvilinear cone intersects the slope ($r_c > r_s$, see Equations (5) and (6) for r_c and r_s), whereas in the former the surface was limited to cases where its center line (Equation (5)) could be tangent to the slope surface, but could not intersect the slope. This limitation was implied by an intuitive conjecture that a critical mechanism will not have "overhanging" regions in the stationary portion of the slope. However, it was found that for some combinations of slope geometry and material properties, the most critical mechanism is one where the center line of the cone intersects the slope ($r_c > r_s$), as indicated in the upper portion of the slope in Figure 1. If an undrained failure is considered, the shape of the failure surface in Figure 1 becomes a torus.

The slope has a stress-free boundary, and the collapsing block rotates as a rigid body; hence, there are only two nonzero terms in Equation (1): the rate of work dissipation D along the failure surface and the rate of work of the soil weight W_γ

$$\int_L T_i\,[v]_i dL = \int_V X_i v_i dV \tag{9}$$

or

$$D = W_\gamma. \tag{10}$$

We first derive an expression for term W_γ. A new algorithm is developed for calculating W_γ in order to include cases with $r_c > r_s$. A general expression can be written as

$$W_\gamma = \int_V \gamma\, v\, \cos\Theta \mathrm{dV} \tag{11}$$

where γ is the soil unit weight, v is the velocity magnitude, θ is the angle between the velocity and the gravity direction, and V is the volume of the rotating block. The infinitesimal volume element shown in Figure 1 (hatched stripe) is calculated as

$$dV = \rho\sqrt{R^2-(\rho-r_c)^2}\,\mathrm{d}\rho\,\mathrm{d}\theta. \tag{12}$$

With velocity magnitude v given by $v = \omega\rho$ (ω- angular velocity about axis through point O) and its direction perpendicular to ρ, one obtains

$$W_\gamma = 2\omega\gamma\int_{\theta_0}^{\theta_h}\int_{r_s}^{r}\rho^2\cos\theta\sqrt{R^2-(\rho-r_c)^2}\,\mathrm{d}\rho\,\mathrm{d}\theta \tag{13}$$

where the lower and upper radial integration limits r_s and r are defined in Equations (6) and (2), respectively. A general expression for the rate of work dissipation along a failure surface can be written as

$$D = \int_L c\,v\cos\phi\,dL \tag{14}$$

where c is cohesion, ϕ is the internal friction angle and L is the area of the failure surface. With the infinitesimal surface element dL (Figure 1)

$$dL = dl\,da = \frac{\rho}{\cos\phi}\frac{R}{\sqrt{R^2-(\rho-r_c)^2}}\mathrm{d}\rho\,\mathrm{d}\theta \tag{15}$$

the rate of work dissipation can be calculated as

$$D = 2c\omega\int_{\theta_0}^{\theta_h}\int_{r_s}^{r}\rho^2\frac{R}{\sqrt{R^2-(\rho-r_c)^2}}\,\mathrm{d}\rho\mathrm{d}\theta \tag{16}$$

where the lower and upper radial limits r_s and r are defined in Equations (6) and (2), respectively. Substituting the expressions in Equations (13) and (16) into Equation (10), one can determine the upper bound to the stability factor defined as

$$N_f = \frac{\gamma\mathrm{H}}{c} \tag{17}$$

or a lower bound to its reciprocal, often referred to as the stability number[3]

$$N_n = \frac{1}{N_f} = \frac{c}{\gamma\mathrm{H}}. \tag{18}$$

The best solution is found through minimization of N_f with angles θ_0, θ_C, θ_h, and ratio r_0'/r_0 being variable. If ratio r_0'/r_0 is restricted to $r_0'/r_0 \geq 0$, the critical mechanism has a finite width, with the critical solution typically when $r_0'/r_0 = 0$. However, it is counterintuitive that a 3D solution would not approach the 2D solution in the absence of any restriction on the width of the failure. The cause of this peculiarity is presumably in that the curvature of the failure surface in the central cross section (Figure 1) is not independent of the curvature in the cross section perpendicular to the plane of Figure 1. To remove this limitation, an alternative mechanism was developed (Michalowski and Drescher[14]), where negative ratio r_0'/r_0 was allowed. The respective mechanism is illustrated in Figure 2. The log-spiral in Equation (3) is now replaced with

$$r'(\theta) = -r_0' e^{(\theta-\theta_0)\tan\phi}. \tag{19}$$

With ratio r_0'/r_0 dropping to large negative numbers, the size of the circular cross section (shaded area in Figure 2A) increases (curvature decreases), whereas the curvature in the plane of symmetry is not coupled with this change. Consequently, the solution to the stability factor approaches an asymptote with a decrease in ratio r_0'/r_0, but this asymptotic solution is not equal to the 2D solution. For example, for a 45° slope and $\phi = 15°$, the asymptotic solution is about $\gamma H/c = 14.11$, whereas the 2D solution is $\gamma H/c = 12.05$.

Based on a different premise (limit equilibrium and variational approach to finding the critical solution), Leshchinsky et al[12] arrived at a similar failure surface, albeit with two distinct restrictions. Although their analysis

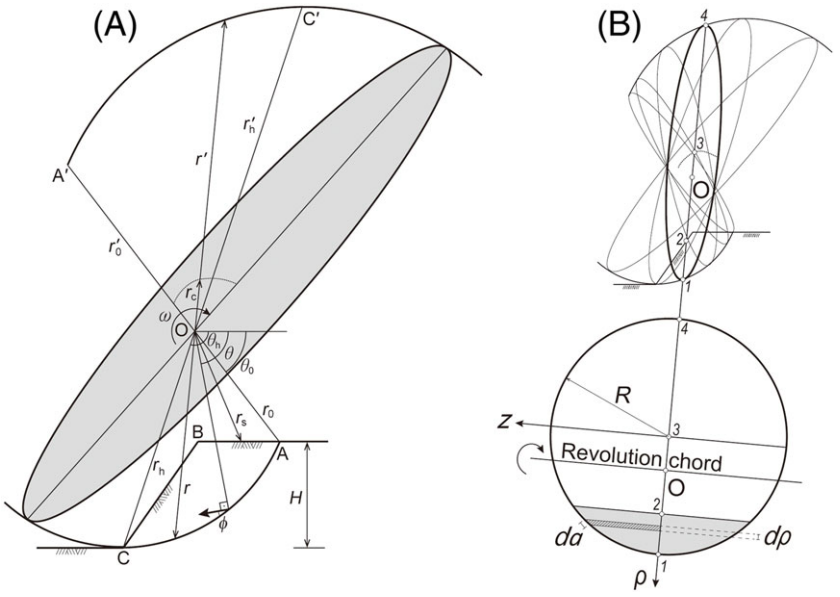

FIGURE 2 Alternative mechanism generated by revolution of a circle with increasing diameter about a chord

included a different set of geometric parameters, the two restrictions, in terms of parameters used in this paper, were: $r_0'/r_0 = 0$, ie, the upper log-spiral in Figure 1 is reduced to a point, and $r_c \leq r_s$, ie, the center line of the curvilinear cone cannot intersect the slope. Leshchinsky et al[12] reported their 3D results in a graph as a stability number (Equation (18)); their solution is compared in Figure 3 with the 3D asymptotic solution calculated based on the alternative mechanism shown in Figure 2, and with the 2D solution. Not surprisingly, the 2D solution yields the more critical outcome than either of the 3D solutions (the higher the stability number the more accurate the result as the kinematic approach yields the lower bound to the stability number in Equation (18)).

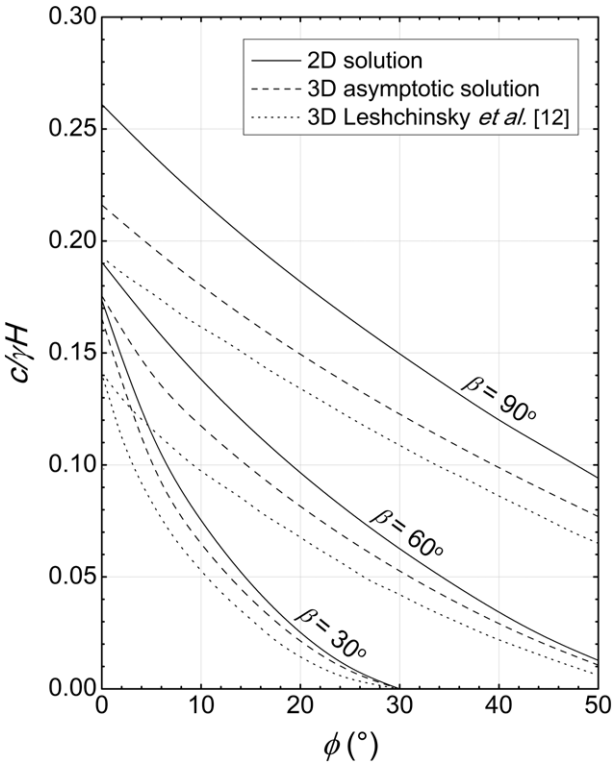

FIGURE 3 Comparison of 3D solutions from Leshchinsky et al[12] to the 3D asymptotic solution in this study based on the alternative mechanism in Figure 2

3.2 | A mechanism with an insert

In order to allow the 3D solution to approach the 2D solution in the absence of restrictions on the size of the mechanism, an insert with 2D geometry is included, as shown in Figure 4. Such a modification was used earlier by Baligh and Azzouz[5] and Leshchinsky and Baker[45] in the limit equilibrium analysis, and also by Michalowski and Drescher[14] in the limit analysis approach. The reader will notice the "overhanging" region in the stationary material when the center line of the curvilinear cone intersects the slope ($r_c > r_s$). The work dissipation and the work rate of the soil weight in the insert were calculated using a well-known procedure,[31] and the respective expressions are not reproduced here. Figure 5 illustrates the trace of three possible variations of the collapse mechanism: toe failure, below-toe failure, and the face collapse. Depending on the limitation on the width of the mechanism, the most critical toe and below-toe mechanisms may include the insert, but the face failure mechanisms never do. This is illustrated in an example solution in Figure 6 for a 60° slope and $\phi = 30°$. Without any limitation on the mechanism width, the failure pattern tends to a 2D mechanism reaching the toe (or below the toe for small slope inclinations). In this particular case, the stability number (Equation (18)) from the 2D solution is 0.062. Once the limitation on the width is imposed, the plane insert in the most critical mechanism is progressively reduced with a drop in the mechanism width (drop in ratio B/H; B—width, H—slope height), until the 2D insert is reduced to zero (at about $B/H = 0.78$). With further decrease in the width of the mechanism, the critical toe mechanism (without insert) slightly changes its shape due to width reduction, until such ratio $(B/H)^*$ where an admissible toe mechanism can no longer be constructed. In this particular example, this occurs at $B/H = 0.65$, beyond which only a face mechanism can fit into the narrow space. This is why the critical face mechanisms do not include plane inserts. The dimensionless width at that transition is defined as $(B/H)^*$, with associated stability number N_n^*. For this specific example: $N_n^* = 0.032$. The stability number for narrower slopes can be simply determined from

$$\frac{c}{\gamma \mathrm{H}} = N_n^* \frac{\dfrac{B}{H}}{\left(\dfrac{B}{H}\right)^*} = N_n^* \left(\frac{H}{B}\right)^* \frac{B}{H} \tag{20}$$

where B/H is the limitation on the slope width ($B/H < (B/H)^*$). Because the starred quantities are constant for a given slope, Equation (20) is linear in B/H, as illustrated by the dashed line in Figure 6. The dots on the dashed line represent independent computations for varying heights h ($h < H$) of the mechanism (see Figure 5 for h).

4 | CALCULATED RESULTS

An upper bound to the stability factor in Equation (17) was calculated using the work rate balance in Equation (10) with the two terms described in Equations (16) and (13). Additionally, the respective terms for the plane insert[31] were added to account for wide mechanisms. The variable parameters in the process of minimizing the stability factor were angles θ_0, θ_h, θ_C (the latter for below-toe failure only), and ratio r_0'/r_0 (see Figure 1). Angles θ_i were varied with a minimum increment of 0.01°, and ratio r_0'/r_0 was varied with a minimum of 0.001. The iteration was stopped when the difference between the two consecutive solutions was less than 10^{-6}. The first set of results is presented in Figure 7. Stability

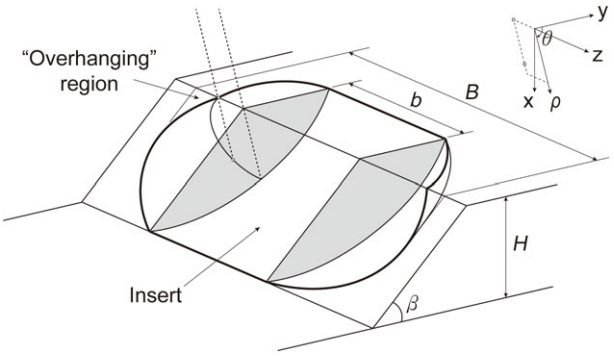

FIGURE 4 Rotational mechanism with an insert with 2D geometry

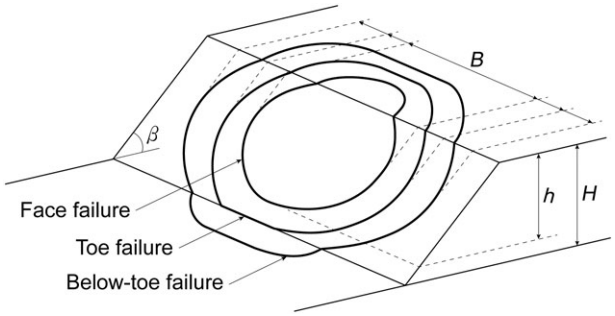

FIGURE 5 Trace of three types of possible failure patterns

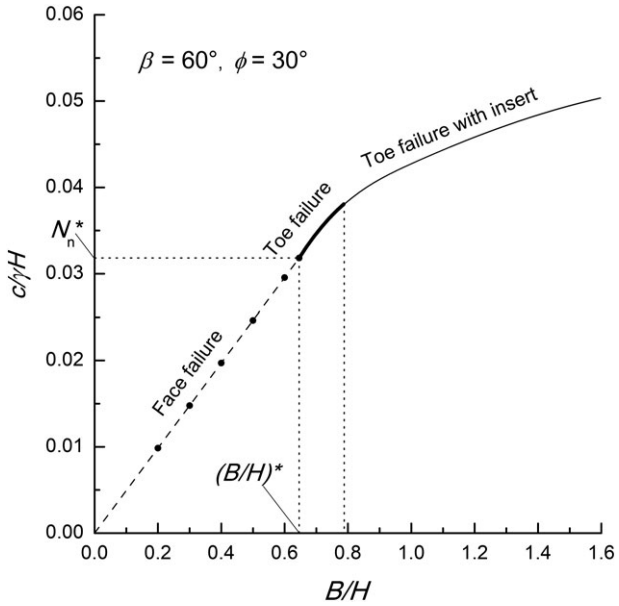

FIGURE 6 Dependence of the failure type on the relative slope width

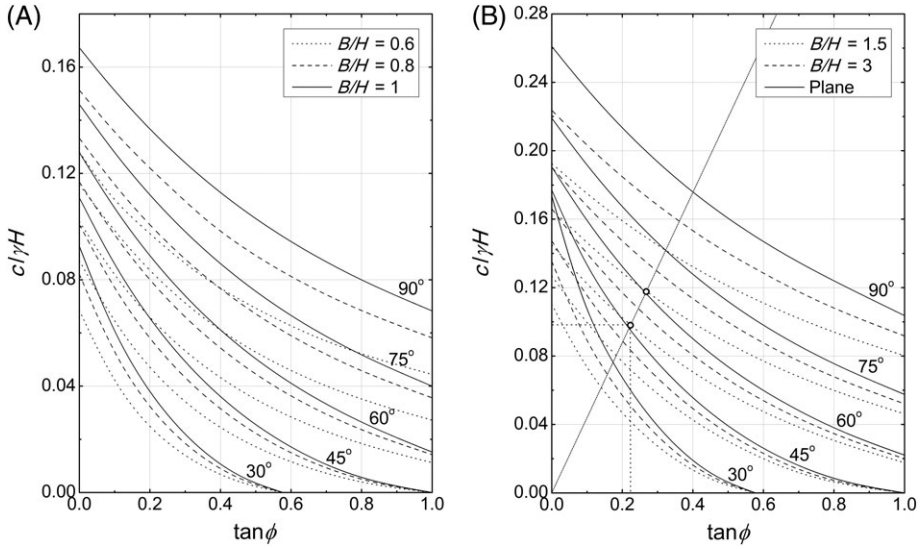

FIGURE 7 Stability number for slopes as function of tanϕ for slopes with inclination 30° to 90°: A, for narrow slopes, $B/H \leq 1.0$, and B, for wide slopes, $B/H \geq 1.5$

TABLE 1 Stability factor $\gamma H/s_u$ for undrained slope failure

		β				
B/H	**Source**	**30°**	**45°**	**60°**	**75°**	**90°**
0.5	This study	16.645	12.789	10.860	9.624	8.753
	Gao et al[17]	22.096[b]	15.654[b]	12.674[b]	11.436[b]	11.102[b]
0.6	This study	14.598	11.464	9.808	8.636	7.808
	Gao et al[17]	20.231[b]	13.354[b]	11.107	9.872	9.310
0.8	This study	12.173[a]	9.918	8.561	7.504	6.609
	Gao et al[17]	15.384[b]	10.741	9.079	8.065	7.231
1	This study	10.797[a]	9.021[a]	7.821	6.852	5.979
	Gao et al[17]	11.885[a]	9.477	8.099	7.165	6.515
1.5	This study	9.068[a]	7.883[a]	6.892	6.023	5.194
	Gao et al[17]	9.443[a]	7.994	6.997	6.159	5.383
	Zhang et al[19]	-	8.000	6.993	6.173	5.405
2	This study	8.229[a]	7.335[a]	6.448	5.629	4.824
	Gao et al[17]	8.615[a]	7.456	6.497	5.698	4.917
	Zhang et al[19]	-	7.407	6.494	5.714	4.950
3	This study	7.389[a]	6.783[ac]	6.022	5.252	4.471
	Gao et al[17]	7.417[a]	6.787[a]	6.042	5.273	4.554
	Zhang et al[19]	-	6.803	6.024	5.291	4.545

[a]Below-toe failure mechanism.

[b]Face failure mechanism.

[c]Alternative mechanism.

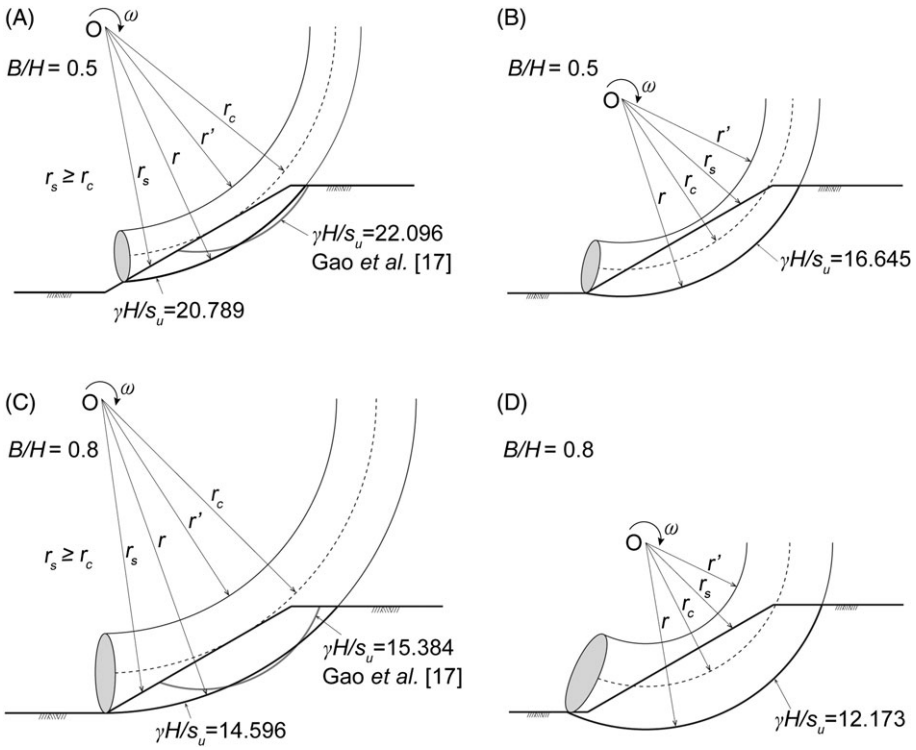

FIGURE 8 Discussion of critical collapse patterns for undrained failure in narrow slopes (slope inclination 30°)

numbers (reciprocal of stability factors) are shown as functions of $\tan\phi$ for slope angles varying from 30° to 90°, and for different limitations B/H on the width of the mechanism. Such presentation is convenient, because it allows for easy reading of the factor of safety F defined as

$$F = \frac{c}{c_d} = \frac{\tan\phi}{\tan\phi_d} \tag{21}$$

where subscript d stands for *developed* (mobilized) strength parameters at failure. This procedure is described briefly in the Appendix.

In the case of undrained failure, the failure surface reduces to a torus. Numerical values of the stability factors for undrained failure $\gamma H/s_u$ are compared in Table 1 to those in Gao et al[17] and Zhang et al[19] (Zhang et al presented numerical values of stability numbers, so they were converted into stability factors). The results given in Gao et al[17] follow the analysis presented originally in Michalowski and Drescher,[14] although Gao et al[17] used a more efficient minimization procedure. The largest difference in the results produced in this paper and those in Gao et al[17] and Zhang et al[19] is for narrow slopes. For instance, for $B/H = 0.5$ and undrained failure, Gao et al[17] overestimate the result in this study by approximately 33% for a gentle slope of 30°, and by approximately 27% for a vertical slope. The largest overestimation of almost 39% was found for a 30° slope and $B/H = 0.6$. However, this overestimation drops to no more than 2%

TABLE 2 Comparison of stability factors $\gamma H/s_u$ for undrained collapse of a 30° slope

					This Study		Gao et al[17]	
B/H	θ_0, °	θ_h, °	θ_c, °[a]	r_0'/r_0	Mode	$\gamma H/s_u$	Mode	$\gamma H/s_u$
0.5[b]	38.42	85.71	-	0.802	Face failure	20.789	Face failure	22.096
0.5	26.05	100.44	-	0.728	Toe failure	16.645	-	-
0.8[b]	41.53	89.14	-	0.747	Toe failure	14.596	Face failure	15.384
0.8	19.42	108.89	114.95	0.541	Below-toe	12.173	-	-

[a]Below-toe failure only, otherwise $\theta_c = \theta_h$.

[b]Constrained solution, $r_s \geq r_c$.

TABLE 3 Stability factor $\gamma H/c$ for $\phi = 15°$

		β				
B/H	Source	30°	45°	60°	75°	90°
0.5	This study	73.120[a]	32.198[a]	20.805[a]	15.946[a]	13.481[a]
	Gao et al[17]	73.156[a]	32.371[a]	21.512[a]	16.580[a]	14.171[a]
0.6	This study	61.008[a]	26.723	17.482	13.391	11.186[a]
	Gao et al[17]	61.014[a]	26.913[a]	17.765[a]	13.727[a]	11.787[a]
0.8	This study	46.071	21.220	14.307	10.939	8.813
	Gao et al[17]	46.101	21.223	14.338	11.074	9.194
1	This study	38.795	18.648	12.786	9.797	7.831
	Gao et al[17]	38.011	18.653	12.831	9.784	8.022
1.5	This study	31.126	15.855	11.087	8.503	6.711
	Gao et al[17]	31.154	15.865	11.120	8.339	6.783
	Zhang et al[19]	-	16.129	11.236	8.475	6.897
2	This study	28.094	14.699	10.363	7.942	6.223
	Gao et al[17]	28.098	14.699	10.363	7.997	6.258
	Zhang et al[19]	-	14.706	10.417	8.000	6.329
3	This study	25.540	13.686	9.714	7.433	5.779
	Gao et al[17]	25.544	13.686	9.716	7.435	5.789
	Zhang et al[19]	-	13.699	9.709	7.463	5.848

[a]Face failure mechanism.

TABLE 4 Stability factor $\gamma H/c$ for $\phi = 30°$

B/H	Source	β			
		45°	60°	75°	90°
0.5	This study	96.342[a]	40.604[a]	25.476[a]	18.952[a]
	Gao et al[17]	96.829[a]	40.801[a]	25.988[a]	19.553[a]
0.6	This study	80.352[a]	33.878[a]	21.232[a]	15.644[a]
	Gao et al[17]	80.678[a]	33.999[a]	21.572[a]	15.304[a]
0.8	This study	62.121	26.464	16.534	11.934
	Gao et al[17]	62.213	26.486	16.659	12.263
1	This study	54.069	23.398	14.647	10.414
	Gao et al[17]	54.193	23.413	14.461	10.503
1.5	This study	45.839	20.216	12.652	8.849
	Gao et al[17]	46.442	20.233	12.709	8.704
	Zhang et al[19]	45.455	20.408	12.821	8.850
2	This study	42.611	18.938	11.836	8.206
	Gao et al[17]	42.625	18.941	11.844	8.212
	Zhang et al[19]	43.478	18.868	11.905	8.333
3	This study	39.866	17.830	11.120	7.635
	Gao et al[17]	39.896	17.832	11.120	7.632
	Zhang et al[19]	40.000	17.857	11.111	7.692

[a]Face failure mechanism.

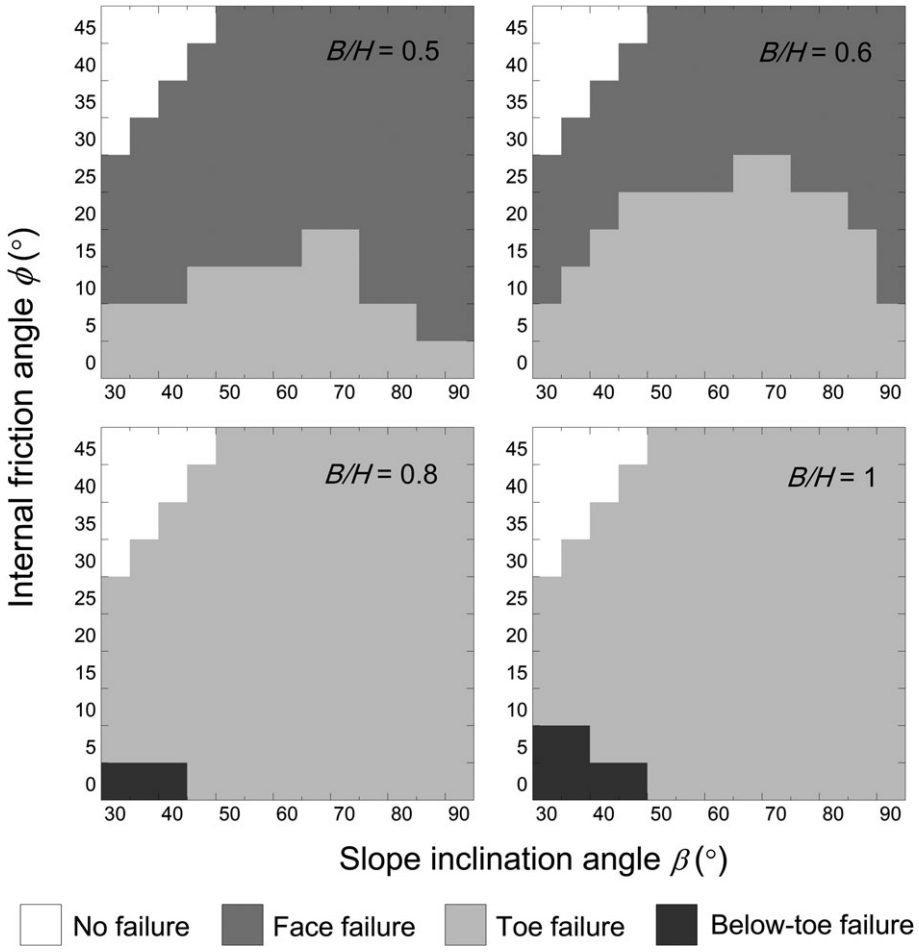

FIGURE 9 Dependence of the failure pattern on the slope inclination and the soil internal friction angle

when $B/H = 3$. Zhang et al (2016) did not report the results for $B/H < 1.5$. Because the kinematic analysis yields an upper bound to the stability factor, the lower estimates in Table 1 are more accurate. The most likely reason for overestimating the results in Gao et al[17] and Zhang et al[19] is excluding mechanisms that would allow the center line of the torus to intersect the slope. This limitation on the geometry of the mechanism was imposed in both papers,[17,19] even though a different method of solution was used. This limitation was also used in the paper of Michalowski and Drescher,[14] but this restriction is relaxed in this study. A graphical illustration of this limitation is presented in Figure 8 using an example of undrained failure of a 30° slope limited to width ratios $B/H = 0.5$ and $B/H = 0.8$. The said limitation can be mathematically described as

$$r_s \geq r_c \tag{22}$$

where r_s is the radius tracing the contour of the slope given in Equation (6), and r_c is the radius of the central line of the torus given in Equation (5). The central line of the torus is traced with a dashed line in Figure 8. The geometry of the failure mechanism for $B/H = 0.5$ is illustrated in Figure 8A,B with the restriction in Equation (22) and without, respectively. The most critical mechanism was found when the restriction in Equation (22) is not enforced; it is a toe mechanism illustrated in Figure 8B, which has the lowest stability factor $\gamma H/s_u = 16.65$. When the constraint in Equation (22) is enforced, the best failure mechanism appears to be a face failure as in Figure 8A, with $\gamma H/s_u = 20.79$. Gao et al's solution

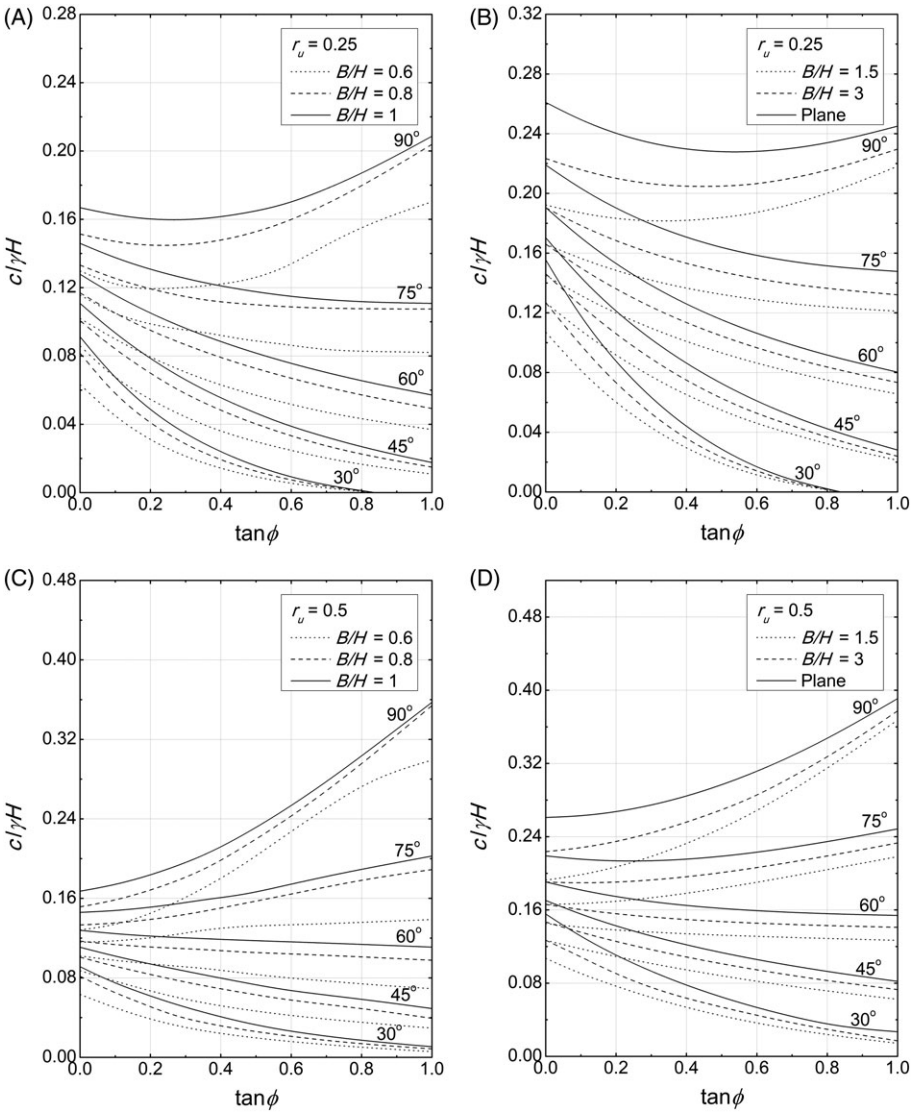

FIGURE 10 Stability number for slopes in the presence of seepage for slopes with inclination 30° to 90°: A, $r_u = 0.25$ and narrow slopes, $B/H \leq 1.0$; B, $r_u = 0.25$ and wide slopes, $B/H \geq 1.5$; C, $r_u = 0.5$ and narrow slopes, $B/H \leq 1.0$; and D, $r_u = 0.5$ and wide slopes, $B/H \geq 1.5$

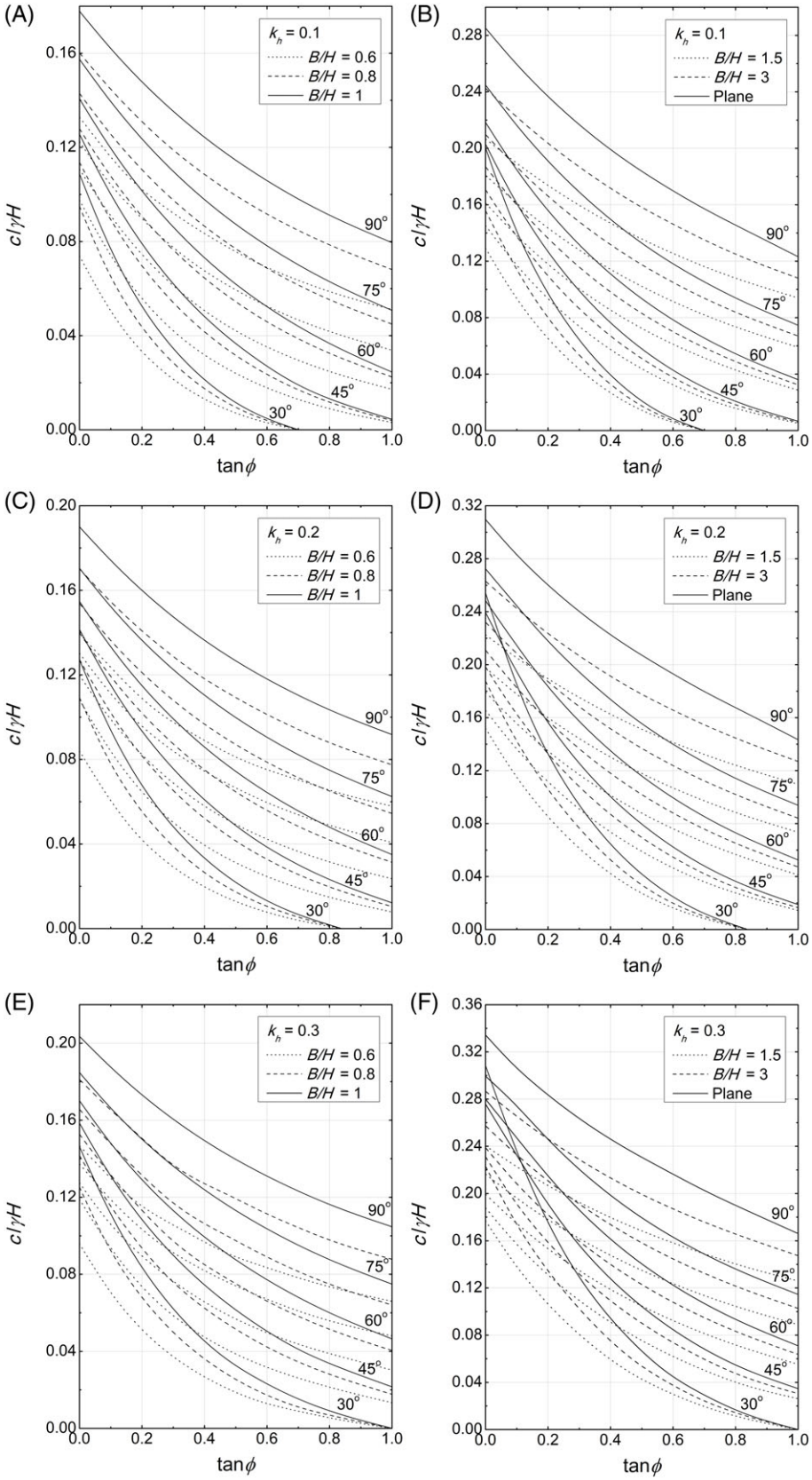

FIGURE 11 Stability number for slopes subjected to horizontal acceleration: A, $k_h = 0.1$ and narrow slopes, $B/H \leq 1.0$; B, $k_h = 0.1$ and wide slopes, $B/H \geq 1.5$; C, $k_h = 0.2$ and narrow slopes, $B/H \leq 1.0$; D, $k_h = 0.2$ and wide slopes, $B/H \geq 1.5$; E, $k_h = 0.3$ and narrow slopes, $B/H \leq 1.0$; and F, $k_h = 0.3$ and wide slopes, $B/H \geq 1.5$

in Gao et al[17] used the limitation in Equation (22), and they found the face failure to be critical, but their solution appears to be less accurate ($\gamma H/s_u = 22.10$, Figure 8A), and it overestimates the best solution in this paper (Figure 8B) by almost 33%. Zhan et al[19] did not produce results for B/H less than 1.5; they only considered mechanisms with an additional limitation $r' = 0$, and only toe failures. Calculations revealed that with these two limitations, one cannot fit an admissible toe mechanism in a narrow slope such as that with a width ratio $B/H = 0.5$.

It is interesting to investigate an undrained failure of a slightly wider 30° slope, $B/H = 0.8$. The most critical mechanism found now is an under-toe failure, $\gamma H/s_u = 12.17$, whereas the solution offered by Gao et al[17] is a face failure with $\gamma H/s_u = 15.38$, a 26% overestimation. If the limitation in Equation (22) is used in the solution offered in this paper, the critical mechanism is a toe failure, and with $\gamma H/s_u = 14.60$ still more accurate than the solution in Gao et al,[17] Figure 8 C. The specific geometric parameters defining the solutions in Figure 8 are given in Table 2. The precision of three digits after the decimal point in all tables is given only for comparative reasons.

Comparisons of stability factors for $\phi = 15°$ and $\phi = 30°$ are presented in Tables 3 and 4. In all cases, the current study provides lower stability factors, but the differences are less than 6% and in many cases less than 1%.

In all results presented in the tables, the least upper bound to the stability factor was reported. Whether this critical solution is a toe failure, below-toe, or a face failure depends on the combination of the slope inclination angle (β), internal friction angle (ϕ), and the slope width limitation (B/H). The three collapse patterns are marked in the graph in Figure 9.

4.1 | An influence of seepage

Previous results were presented for slopes with no seepage. In the absence of known specific hydraulic conditions, coefficient r_u (Bishop and Morgrnstern[46]) is used as a generic means to compare the influence of the presence of pore water pressure for different slopes. This coefficient yields the distribution of the pore water pressure, and the work of this pore water pressure on the volumetric strain of the soil during plastic deformation can be proved to be equal to the work of the buoyancy and the seepage forces.[47,48] Because the plastic deformation occurs only along the failure surface in the mechanism considered, the rate of work of the pore water pressure W_u on the volumetric strain of the soil can be calculated as

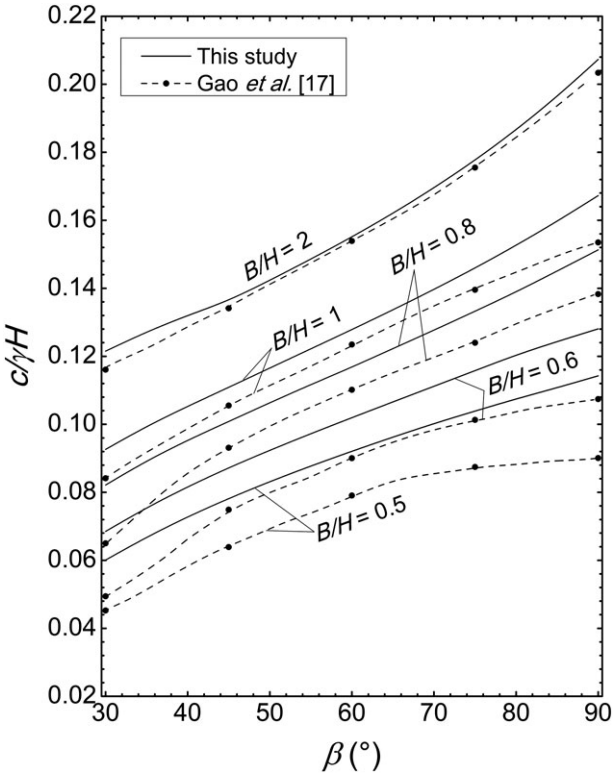

FIGURE 12 Comparison of calculated stability numbers to those in Gao et al[17] for slopes of different widths

$$W_{\mathrm{u}} = \int_L uv \sin\phi \, dL \tag{23}$$

where u is the pore water pressure determined from given coefficient r_u, v is the magnitude of velocity jump vector on the failure surface, ϕ is the internal friction, and L is the area of the failure surface. The expression in Equation (23) was included on the right-hand side of the balance in Equation (10), and the results of calculations are shown in Figure 10.

4.2 | An influence of quasi-static seismic force

Although considering the seismic effects requires dynamics computations, a rough estimate of the vulnerability of slopes to seismic shaking can be considered using a quasi-static approach where the dynamic effects are substituted with a static horizontal load. The intensity of this load is defined by the coefficient of horizontal acceleration k_h. The seismic influence is then included as additional work done by inertial forces. This rate of work, W_S, can be calculated analogously to the rate of soil weight in Equation (11)

$$W_S = k_h \int_V \gamma v \sin\theta \, dV \tag{24}$$

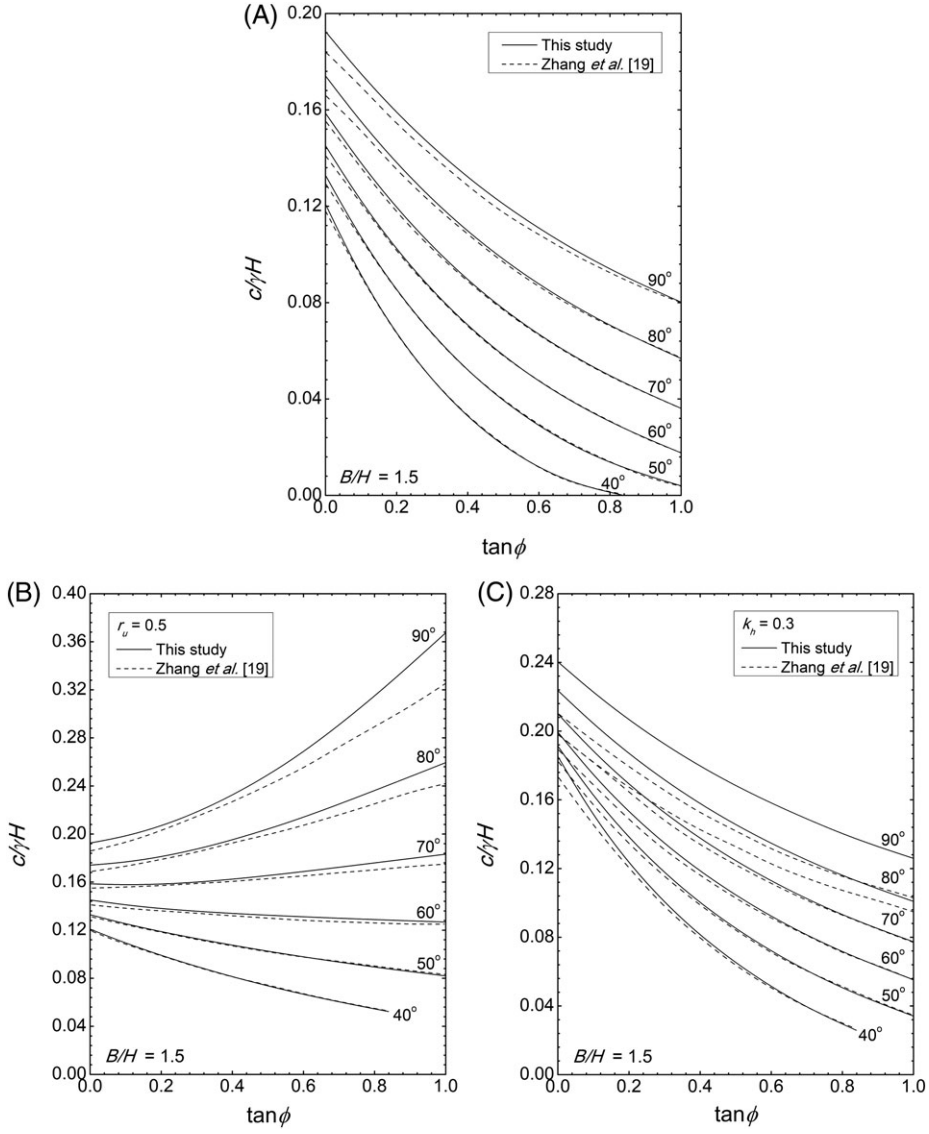

FIGURE 13 Comparison of calculated stability numbers to those in Zhang et al[19] for selected seepage and seismic acceleration, for $B/H = 1.5$

This term was included on the right side of the work rate balance in Equation (10), and the results of computations are illustrated in Figure 11.

5 | DISCUSSION

Kinematic limit analysis is an effective method to assess safety of slopes. Its limitations come from difficulties in considering non-homogeneities in material properties and complex geometries of slopes. Numerical approaches are more efficient in these cases, eg, Li et al,[25] but for simple slopes, the approach presented in this paper typically yields better results.[15,19]

The focus of the discussion is on the sources of discrepancies in the solution results presented in the literature, solutions that come apparently from considering the same failure mechanism. The results based on the procedure presented in this paper were compared with those of Gao et al[17] in Section 4. Their results were based on the same algorithm as

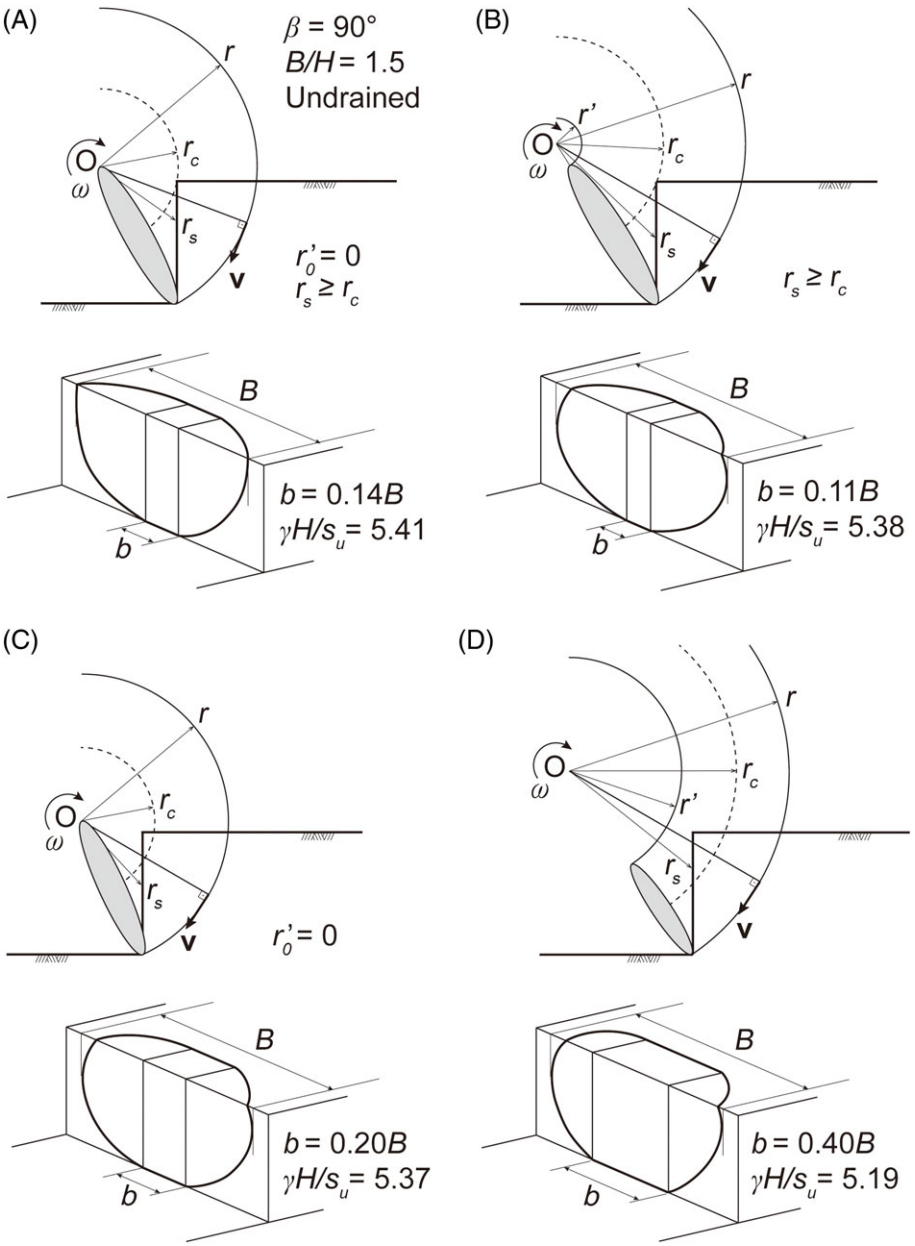

FIGURE 14 Explanation of the impact of geometrical limitations on the outcome of the analysis

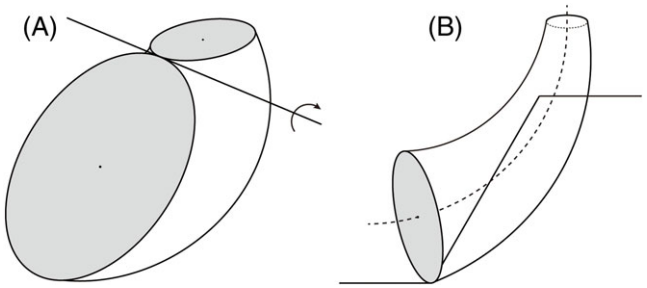

FIGURE 15 A, The shape of a failure surface with limitation $r' = 0$ and B, failure surface allowing $r' > 0$, and also permitting the center line (dashed) to intersect the slope

that in Michalowski and Drescher.[14] The largest discrepancies, up to 39%, were found for narrow slopes failing in an undrained manner. The differences, however, became less significant with an increase in the width of the mechanism of failure and with an increase in the internal friction angle. More comprehensive comparison is presented graphically in Figure 12. The results were presented in Gao et al [17] in terms of the stability factor, and they were converted to the stability number in order to have all graphs presented in a consistent manner (the bullets are the converted numerical values of stability factors and the dashed lines are converted from the graphs in Gao et al[17]).

Zhang et al[19] have not presented results for narrow slopes, where the discrepancies between the results produced in this paper and those in Gao et al[17] were found to be the largest. Their considerations were subject to three constraints: $r' = 0$, $r_s \geq r_c$ (see Figure 1 for r', r_s, and r_c), and toe failures only. With these constraints, one cannot fit admissible rotational mechanisms in narrow slopes, eg, $B/H = 0.5$. The comparison in Figure 13 is then presented for $B/H = 1.5$, the smallest width for which the results were reported in Zhang et al.[19]

When slopes are not subjected to seismic loads, a substantial difference occurs only for very steep slopes failing in an undrained manner. If substantial seepage is accounted for ($r_u = 0.5$), the considerable difference occurs for very steep slopes and large internal friction angles. When slopes are subjected to seismic loads, the results for steep slopes failing in undrained process show the largest discrepancy. In all cases, the analysis presented in this paper provides more accurate results (the kinematic approach yields the lower bound to the stability number, thus the larger the stability number the more accurate the solution).

To reveal the causes of discrepancies among different solutions, we consider the influence of assumptions used in different analyses on the geometry of the critical mechanisms and on the outcome in terms of the stability factor. Consider an undrained failure of a vertical slope with width defined by $B/H = 1.5$. The two graphs (upper and lower) in Figure 14A present a cross section of the critical mechanism from the analysis where the inner diameter of the torus was set to zero, $r' = 0$, and the center line of the torus was not to intersect the slope, $r_s \geq r_c$. With these limitations, the algorithm proposed in this paper converged to a minimum of $\gamma H/s_u = 5.41$, which is equivalent to a stability number (reciprocal of stability factor) equal to 0.185. This is exactly the result reported in Zhang et al,[19] where the authors used the two restrictions. The center line of the torus forming the failure surface is tangent to the slope crest, which is enforced by limitation $r_s \geq r_c$. The solution illustrated in Figure 14B was obtained when limitation $r' = 0$ was relaxed, but the restraint $r_s \geq r_c$ was still enforced. The solution is now improved, with $\gamma H/s_u = 5.38$, the same stability factor as reported in Gao et al[17] where the same limitations were used. If limitation $r_s \geq r_c$ is relaxed, but the inner radius of the torus is set to zero, $r' = 0$, the solution becomes $\gamma H/s_u = 5.37$ (Figure 14C), but the best solution is obtained when both restrictions on the geometry are removed, as in Figure 14D, where $\gamma H/s_u = 5.19$. In this particular case, the numbers reported in Gao et al and Zhang et al[17,19] overestimate the result calculated in this study by only a little more than 4%, but the difference becomes much larger for narrower slopes, as shown in Table 1.

6 | CONCLUSIONS

The geometry of the mechanism postulated in the kinematic approach of limit analysis for assessing the safety of slopes plays a crucial role. While construction of mechanisms with two-dimensional geometry is relatively straightforward, three-dimensional (3D) mechanisms can be intricate due to their complicated geometry. 3D rotational mechanisms with a failure surface in a shape of a curved cone, or a torus for undrained failures, have been used in past studies. It was

demonstrated in this paper that two assumptions used in previous studies of 3D slope failures lead to limitations that exclude the most critical failure mechanisms for some range of slope parameters.

An early example of a rotational 3D collapse pattern was described by Leshchinsky et al,[12] and it was derived by a variational approach used as a means of finding the most critical mechanism. A more general class of admissible failure surfaces can be defined as curvilinear cones, or "horn-shape" surfaces. They can be generated by rotating a circle of increasing diameter about an axis.[14] The surface found in Leshchinsky et al[12] is a special case of such a surface when the axis about which the generating circle revolves is tangent to the circle, Figure 15A, which is a limitation on the multiplicity of admissible surfaces. The second limitation found in earlier analyses[14,17] was in the requirement that the center line of the generated surface would not intersect the slope. These limitations affected the assessment of slope safety and also did not allow finding admissible 3D collapse mechanisms for narrow slopes. The mechanism in the paper by Michalowski and Drescher[14] was independently postulated based on admissibility of the kinematic field; this mechanism was later adopted by others.[17] Although the mechanisms in Leshchinsky et al[12] and Michalowski and Drescher[14] are based on different premises, their geometry is essentially the same, with the exception of the limitations already mentioned. Zhang et al,[19] who more recently presented both approaches, pointed out that an improvement of the results due to removing the first limitation is negligible for wider slopes ($B/H \geq 1.5$). In the study presented in this paper, both limitations were removed, Figure 15B (also 8D and 14D), and it was found that these restrictions have very significant consequences for narrow slopes. The largest difference was found for an undrained failure of a narrow slope with $B/H = 0.6$; the stability factor found by Gao et al[17] overestimates the one in this study by almost 39% (Table 1). Such a large difference was found because removing both limitations widens the range of slope parameters for which admissible failure mechanisms can be found. In general, substantial differences exist for undrained failures in narrow slopes ($B/H \leq 1.0$). The study by Zhang et al[19] did not produce solutions for narrow slopes, because only toe failures were sought, and with the limitations imposed on the geometry of the slope collapse, admissible rotational mechanisms could not be found. The comparisons of results produced in this study and those from previous studies allow concluding that the discrepancies among published results for 3D slope stability analyses come from limitations imposed on the collapse mechanisms used in some of the approaches.

The solution discussed in this paper falls under the category of semi-analytical as the numerical calculations were only used in the optimization phase of the analysis. The numerical approach using finite elements in limit analysis[49,50] is a method that has some advantages over the semi-analytical approach; for example, geometric complexities and material non-homogeneities are easier to account for. However, the solutions to homogeneous slopes with simple geometry appear to be more accurate when using the semi-analytical approach, as demonstrated in Zhang et al.[19] This appears to be true also for other limit-state geotechnical problems.[27]

ACKNOWLEDGEMENTS

The work presented in this paper was carried out when the authors were supported by the National Science Foundation through grant no. 1537222 from the Division of Civil, Mechanical, and Manufacturing Innovation. This support is gratefully acknowledged.

ORCID


Radoslaw L. Michalowski http://orcid.org/0000-0002-9557-4802

REFERENCES

1. Collin A. *Recherches Expérimentales sur les Glissements Spontantés des Terrains argileux.* Paris: Carilian-Goeury; 1846 160 p. Translation by W.R. Schriever: Landslides in Clays. University of Toronto Press, 1956.
2. Fellenius W. *Erdstatische Berechnungen mit Reibungund und Kohäsion (Adhäsion) und unter Annahme kreiszylindrischer Gleitflächen*. Berlin: Ernst & Sohn; 1927 40 p. Translation from the Swedish edition, Stockholm 1926.
3. Taylor DW. *Stability of Earth Slopes*. J. Boston Society of Civil Engineers; 1937 24, No. 3. Reprinted in: Contributions to Soil Mechanics 1925 to 1940. Boston Society of Civil Engineers, 337–386.
4. Drucker DC, Prager W. Soil mechanics and plastic analysis or limit design. *Quart Appl Math*. 1952;10(2):157-165.
5. Baligh MM, Azzouz AS. End effects on stability of cohesive slopes. *ASCE J Geot Eng Div*. 1975;101:1105-1117.

6. Gens A, Hutchinson JN, Cavounidis S. Three-dimensional analysis of slides in cohesive soils. *Géotechnique*. 1988;38(1):1-23.
7. Hovland HJ. Three dimensional slope stability analysis method. *J Geotech Eng Div*. 1977;103:971-986.
8. Hungr O. An extension of Bishop's simplified method of slope stability analysis to three dimensions. *Géotechnique*. 1987;37(1):113-117.
9. Lam L, Fredlund DG. A general limit equilibrium model for three-dimensional slope stability analysis. *Can Geotech J*. 1993;30(6):905-919.
10. Drescher A. Limit plasticity approach to piping in bins. *J Appl Mech*. 1983;50(3):549-553.
11. Michalowski RL. Three-dimensional analysis of locally loaded slopes. *Géotechnique*. 1989;39(1):27-38. https://doi.org/10.1680/geot.1989.39.1.27
12. Leshchinsky D, Baker R, Silver ML. Three dimensional analysis of slope stability. *Int J Num Analyt Meth Geomech*. 1985;9(3):199-223.
13. De Buhan P, Garnier D. Three dimensional bearing capacity analysis of a foundation near a slope. *Soils Found*. 1998;38(3):153-163.
14. Michalowski RL, Drescher A. Three-dimensional stability of slopes and excavations. *Géotechnique*. 2009;59(10):839-850.
15. Michalowski RL. Limit analysis and stability charts for 3D slope failures. *J Geotech Geoenv Eng*. 2010;136(4):583-593.
16. Michalowski RL, Martel T. Stability charts for 3D failures of steep slopes subjected to seismic excitation. *J Geotech Geoenv Eng*. 2011;137(2):183-189.
17. Gao YF, Zhang F, Lei GH, Li DY. An extended limit analysis of three-dimensional slope stability. *Géotechnique*. 2013;63(6):518-524.
18. Nadukuru SS, Michalowski RL. Three-dimensional displacement analysis of slopes subjected to seismic loads. *Can Geotech J*. 2013;50(6):650-661.
19. Zhang F, Leshchinsky D, Baker R, Gao Y, Leshchinsky B. Implications of variationally derived 3D failure mechanism. *Int J Numer Anal Methods Geomech*. 2016;40(18):2514-2531.
20. Bekaert A. Improvement of the kinematic bound for the stability of a vertical cut-off. *Mech Res Com*. 1995;22(6):533-540.
21. Griffiths DV, Marquez RM. Three-dimensional slope stability analysis by elasto-plastic finite elements. *Géotechnique*. 2007;57(6):537-546.
22. Borja RI, Liu X, White JA. Multiphysics hillslope processes triggering landslides. *Acta Geotechnica*. 2012;7(4):261-269.
23. Camargo J, Velloso RQ, Vargas EA. Numerical limit analysis of three-dimensional slope stability problems in catchment areas. *Acta Geotechnica*. 2016;11(6):1369-1383.
24. Hicks MA, Li Y. Influence of length effect on embankment slope reliability in 3D. *Int J Numer Anal Methods Geomech*. 2018;42:891-915.
25. Li AJ, Merifield RS, Lyamin AV. Three-dimensional stability charts for slopes based on limit analysis methods. *Can Geotech J*. 2010;47(12):1316-1334.
26. Lim K, Li AJ, Lyamin AV. Three-dimensional slope stability assessment of two-layered undrained clay. *Comput Geotech*. 2015;70:1-17.
27. Michalowski RL. Collapse loads over two-layer clay foundations soils. *Soils Found*. 2002;42(1):1-7.
28. Tun YW, Llano-Serna MA, Pedroso DM, Scheuermann A. Multimodal reliability analysis of 3D slopes with a genetic algorithm. *Acta Geotechnica*. 2018. https://doi.org/10.1007/s11440-018-0642-9
29. Hill R. *Mathematical Theory of Plasticity*. Oxford: Clarendon Press; 1950:355.
30. Salençon J. *Applications of the Theory of Plasticity in Soil Mechanics*. (Translated from 1974 French edition.). 1977 New York, Wiley:158.
31. Chen WF. *Limit Analysis and Soil Plasticity*. Amsterdam: Elsevier; 1975:638.
32. Mróz Z. Non-associated laws in plasticity. *J Mécanique*. 1963;2:21-42.
33. Radenkovic D. Théorie des charges limites extension a la mécanique des sols. Séminaire de Plasticité. *École Polytechnique*, Publications Scientifiques et Techniques du Ministère de L'Air 1961; Published. 1962;129-141.
34. Palmer AC. A limit theorem for materials with nonassociated flow law. *J Mécanique*. 1966;5:217-222.
35. Collins IF. The upper bound theorem for rigid/plastic solids generalized to include Coulomb friction. *J Mech Phys Solids*. 1969;7:323-338.
36. Mróz Z, Drescher A. Limit plasticity approach to some cases of flow of bulk solids. *ASME J Eng Ind*. 1969;91(2):357-364.
37. Michalowski RL, Mróz Z. Associated and non-associated sliding rules in contact friction problems. *Arch Mech Stos (Archives of Mechanics)*. 1978;30:259-276.
38. Drescher A, Detournay E. Limit load in translational failure mechanisms for associative and non-associative materials. *Géotechnique*. 1993;43(3):443-456.
39. Salençon J. An introduction to the yield design theory and its applications to soil mechanics. *Eur J Mech, A/Solids*. 1990;9:477-500.
40. Hoek E, Bray JW. *Rock Slope Engineering*. 2nd ed. London: Institution of Mining and Metallurgy; 1981:360.
41. Michalowski RL. Upper-bound load estimates on square and rectangular footings. *Géotechnique*. 2001;51(9):787-798.
42. Yang X, Li Z. Kinematical analysis of 3D passive earth pressure with nonlinear yield criterion. *Int J Numer Anal Methods Geomech*. 2018;42(7):916-930.
43. Park D, Michalowski RL. Three-dimensional stability analysis of slopes in hard soil/soft rock with tensile strength cut-off. *Engineering Geology*. 2017;229:73-84.

44. Park D, Michalowski RL. A cone surface in 3D analyses of slopes with tension cut-off. *Geotech Res*. 2018;5(2):51-67.
45. Leshchinsky D, Baker R. Three-dimensional slope stability: end effects. *Soils Found*. 1986;26(4):98-110.
46. Bishop AW, Morgenstern N. Stability coefficients for earth slopes. *Géotechnique*. 1960;10(4):129-150.
47. Michalowski RL. Slope stability analysis: a kinematical approach. *Géotechnique*. 1995;45(2):283-293.
48. Viratjandr C, Michalowski RL. Limit analysis of slope instability caused by partial submergence and rapid drawdown. *Canad Geotech J*. 2006;43(8):802-814.
49. Pastor J. Analyse limite: determination numerique de solutions statiques completes. Application au talus vertical. *J Mech Appl*. 1978;2:167-196.
50. Sloan SW. Upper bound limit analysis using finite elements and linear programming. *Int J Num Analyt Meth Geomech*. 1989;13(3):263-282.
51. Michalowski RL. Stability charts for uniform slopes. *J Geotech Geoenv Eng*. 2002;128(4):351-355.

How to cite this article: Park D, Michalowski RL. Intricacies in three-dimensional limit analysis of earth slopes. *Int J Numer Anal Methods Geomech*. 2018;42:2109–2129. https://doi.org/10.1002/nag.2846

APPENDIX

The stability factor or stability number in Equation (17) or (18) is often used as the means of assessment of the slope safety, but more often the factor of safety in Equation (21) is required in geotechnical design. Extracting the factor of safety from the stability factor (or stability number) typically requires an iterative procedure (except in cases of undrained collapse). A convenient manner of presenting the results without the need for iterations was shown earlier.[51] An alternative way is illustrated here, where the stability number is reported as a function of $\tan\phi$, as in Figures 7, 10, and 11. Inferring the factor of safety from the graphs is explained in an example illustrated in Figure 7B.

Consider a 10-m tall (H) slope, 15 m in width (B), with inclination angle of 60° (β), and the following material properties: $\gamma = 17$ kN/m^3, $c = 20$ kN/m^2, and $\phi = 15°$. Hence, $\tan\phi = 0.268$ and the noncritical dimensionless group $c/\gamma H$ for this (safe) slope is 0.118. Now, mark a point on the graph with coordinates 0.268 and 0.118 (upper open circle), and draw a straight line through it and the origin of the chart. Find the intersection point of this line with the curve for $\beta = 60°$ and $B/H = 1.5$ (lower open circle). The ratio of the length from the origin to the upper circle to the length connecting the origin and the lower circle is the factor of safety; in this case F $\approx$ 1.20.